ELSEVIER

Contents lists available at ScienceDirect

Journal of Biomechanics

journal homepage: www.elsevier.com/locate/jbiomech





Aortic tissue stiffness and tensile strength are correlated with density changes following proteolytic treatment

Pete H. Gueldner ^a, Cyrus J. Darvish ^a, Isabelle K.M. Chickanosky ^a, Emma E. Ahlgren ^b, Ronald Fortunato ^b, Timothy K. Chung ^{a,i}, Keshava Rajagopal ^c, Chandler C. Benjamin ^d, Spandan Maiti ^a, Kumbakonam R. Rajagopal ^{a,d}, David A. Vorp ^{a,b,e,f,g,h,i,*}

- ^a Department of Bioengineering, University of Pittsburgh, Pittsburgh, PA, USA
- ^b Department of Mechanical Engineering and Materials Science, University of Pittsburgh, Pittsburgh, PA, USA
- ^c Department of Cardiac Surgery, Jefferson University, Philadelphia, PA, USA
- d Department of Mechanical Engineering, Texas A&M University, College Station, TX, USA
- ^e McGowan Institute for Regenerative Medicine, University of Pittsburgh, Pittsburgh, PA, USA
- f Department of Surgery, University of Pittsburgh, Pittsburgh, PA, USA
- g Department of Chemical and Petroleum Engineering, University of Pittsburgh, Pittsburgh, PA, USA
- ^h Department of Cardiothoracic Surgery, University of Pittsburgh, Pittsburgh, PA, USA
- ⁱ Clinical and Translational Sciences Institute, University of Pittsburgh, Pittsburgh, PA, USA

ABSTRACT

Introduction: Dissection or rupture of the aorta is accompanied by high mortality rates, and there is a pressing need for better prediction of these events for improved patient management and clinical outcomes. Biomechanically, these events represent a situation wherein the locally acting wall stress exceed the local tissue strength. Based on recent reports for polymers, we hypothesized that aortic tissue failure strength and stiffness are directly associated with tissue mass density. The objective of this work was to test this novel hypothesis for porcine thoracic aorta.

Methods: Three tissue specimens from freshly harvested porcine thoracic aorta were treated with either collagenase or elastase to selectively degrade structural proteins in the tissue, or with phosphate buffer saline (control). The tissue mass and volume of each specimen were measured before and after treatment to allow for density calculation, then mechanically tested to failure under uniaxial extension.

Results: Protease treatments resulted in statistically significant tissue density reduction (sham vs. collagenase p=0.02 and sham vs elastase p=0.03), which in turn was significantly and directly correlated with both ultimate tensile strength (sham vs. collagenase p=0.02 and sham vs elastase p=0.03) and tangent modulus (sham vs. collagenase p=0.007 and sham vs elastase p=0.03).

Conclusions: This work demonstrates for the first time that tissue stiffness and tensile strength are directly correlated with tissue density in proteolytically-treated aorta. These findings constitute an important step towards understanding aortic tissue failure mechanisms and could potentially be leveraged for non-invasive aortic strength assessment through density measurements, which could have implications to clinical care.

1. Introduction

Normal physiologic functioning of the cardiovascular system depends on the ability of the vascular tissues to safely bear imposed hemodynamic loading. A loss of biomechanical integrity of the vascular tissue often leads to catastrophic clinical events. For example, rupture of abdominal aortic aneurysm and dissection of a thoracic aortic aneurysm are caused by mechanical failure of the aortic wall tissue and results in death up to 90% and to 43% of the time, respectively (Gloviczki et al., 1992; Lau et al., 2019). Elective surgical intervention of aortic aneurysms is currently based on the maximum diameter criterion (Darling

et al., 1977; Lombardi et al., 2020), which is inadequate as currently up to 13% and 2% of the patients, respectively, with aneurysms below the surgical threshold diameter do experience this clinical event (Davies et al., 2002; Kontopodis et al., 2016). Therefore, a pressing need exists for better evidence-based metrics to predict rupture and dissection risk for improved patient management and clinical outcome.

From a biomechanics perspective, an aortic rupture or dissection event is a mechanical failure of the aortic tissue when local aortic wall stress exceeds the local wall strength (Siika et al., 2023; Thunes et al., 2018; Vande Geest et al., 2006a). Therefore, a non-invasive means to accurately predict local wall strength could prove valuable in prediction

https://doi.org/10.1016/j.jbiomech.2024.112226

^{*} Correspondence author at: John A. Swanson Professor of Bioengineering, USA (David A. Vorp,). E-mail address: vorp@pitt.edu (D.A. Vorp).

of risk that a given aneurysm is under with respect to these events. While many experimental studies have been performed to quantify aneurysmal tissue strength (Di Martino et al., 2006; Duprey et al., 2016; Mohan and Melvin, 1983; Raghavan et al., 1996; Vande Geest et al., 2006b; Vande Geest et al., 2006c; Vorp, 2007) and have provided valuable data about the failure properties of aortic tissue, biomechanical pathways controlling the failure process remain to be explored.

Our understanding of soft tissue failure modes and mechanisms is still in its early stage, however. Some earlier efforts attempted to apply isotropic (Karimi et al., 2014; Volokh, 2011; Volokh and Vorp, 2008; Vorp et al., 1998) and anisotropic material failure theories (Gasser et al., 2006; Korenczuk et al., 2017) to better understand failure of soft tissues, including the aorta. More recently we reported an AI-based method to predict the mechanical yield point in aneurysmal and non-aneurysmal abdominal aorta (Chung et al., 2024). Traditional failure theories typically utilize a measure of stress (or strain) as the determiner of failure initiation within a material (Hinton et al., 2004; Özkaya et al., 2016). However, such theories are difficult to apply to loaded soft tissues, in which we do not know the *in-vivo* reference stress, and thus, the absolute stress state (Fung and Liu, 1991; Fung, 1991; Gee et al., 2009; Liu and Fung, 1988, 1989; Lu et al., 2007; Sokolis, 2015; Sokolis et al., 2023)). Damage-based modeling of soft tissue failure has been reported (Ferreira et al., 2017; Mousavi et al., 2018; Rausch et al., 2017). While these efforts have advanced our knowledge of tissue failure phenomena, they treat materials as homogeneous and use values of stress or strain as the determiner of damage initiation. Soft tissues are inherently heterogeneous, including variations of mass density from point to point, and this should be accounted for in development of theories pertinent to tissue

Aortic tissue is highly heterogeneous, consisting of a network of collagen and elastin as its primary mechanical load-bearing constituents. Prior studies have shown elevated stiffness, higher volume fraction of collagen, and lower amounts of elastin in aneurysmal compared to healthy aortas (He and Roach, 1994). The lower amount of elastin is associated with the degenerative process which accompanies the ballooning/distension of the aneurysm (Dobrin et al., 1988). Treatments with collagenase and elastase (amongst other proteins) have been used to recreate the aneurysmal environment in-vivo in mouse (Berman et al., 2022; Gueldner et al., 2023) and rat (Marbacher et al., 2014) models and reported an overall decrease in tissue strength. While these reports corroborate the load bearing and strength-providing functions of the tissue fiber network in aorta, primary parameters of the network determining biomechanical failure remain largely unknown. However, this knowledge is critical for gaining mechanistic insight into tissue failure properties that ultimately dictate aortic dissection or rupture.

We hypothesize that the origin of tissue damage, the precursor to soft tissue failure, can be attributed to a reduction in the tissue density rendering the tissue more susceptible to failure. The premise of this hypothesis is based on the recent work of Alagappan et al., who successfully predicted experimental failure behavior of different engineered soft materials by attributing the origin of damage and fatigue to material density reduction in the test specimens (Alagappan et al., 2016; Alagappan and Rajagopal, 2022, 2023; Alagappan et al., 2018a,b). In this article, we sought to test our hypothesis by determining how reduction in bulk material density influences the failure behavior of porcine thoracic aortic tissue.

2. Methods

2.1. Porcine aortic specimen preparation

A total of 7 porcine thoracic aortas were collected freshly from a local abattoir (Thoma Meat Market, Saxonburg, PA). The pigs were male, 6–9 months old, Yorkshire, and approximately 300 lb. All aortas were kept on ice during transport to the laboratory, where individual tissue strip specimens were cut and placed in cold phosphate buffered saline (PBS)

for storage to prevent tissue degradation. To cut individual specimens, a die stamp was 3D printed using a Guider II printer (Flashforge, Zhejiang, China). Flexible barber blades (Derby Professional, Newton Center, MA) were clamped inside the stamp to cut dumbbell-shaped sections (an idea adapted from (Nelson et al., 2020)). The die was made to cut specimens 60 mm long total with a 40 mm gauge length and 4 mm wide in the central region with 10 mm wide heads on either end. The thoracic aortic segments were longitudinally cut and 3 dumbbell sections were stamped from same axial position (Fig. 1A), avoiding posterior regions containing vertebral arteries. Each specimen was then stored in PBS for a few hours at room temperature to allow for tissue saturation. The three specimens were then treated with either PBS (sham), collagenase, or elastase as described below. It is important to note that our use of protease treatment on healthy aortic tissue was not to mimic aneurysmal tissue, but rather as a means to alter the tissue density for testing our hypothesis.

2.2. Mass and volume measurements and bulk density calculation

The bulk tissue density was taken as the ratio of the mass and volume and was measured individually for each mechanical test specimen prior to treatment (Fig. 1B). Specimens were first incubated in PBS for an hour at 37 °C, dabbed to remove surface moisture, then mass was determined using a precision balance (PR503, Mettler Toledo, Columbus, OH) and volume was determined using two different techniques to gather porefree and spatial volumes. The "pore-free volume" (Fig. 2A) was measured from fluid displacement, which considers all solids and fluids within the tissue, but fills the pores with fluid. The volume of fluid in a 10 mL graduated cylinder was noted, and the specimens were added. The volume was remeasured, and the pore-free volume was acquired by subtracting the two measures. The "spatial volume" (Fig. 2B) considers the solid, fluid, and pores as the solid object, that is, the total encapsulated space occupied by the specimen. The surface area was measured by optically imaging the top of the specimens with an in-plane ruler and delineating the boundary of the samples defining the surface using a custom MATLAB (v R2022a, Mathworks, Natick, MA) script. The spatial volume (V) was then calculated from the measured surface area (SA) and average thickness (t) across the specimens, where V = SA*t.

2.3. Collagenase and elastase treatments

After the mass and volume were measured, the samples were placed in a rotating incubator (37 $^{\circ}$ C) tray and treated for 24 h with PBS (sham), 70 mg/ml collagenase solution (Collagenase Type 3, Worthington, Columbus, OH, USA) or 0.01 mg/ml elastase solution (Purified Lyophilized Elastase, Worthington, Columbus, OH, USA) (Fig. 1C). The treatment time and concentrations were determined through trial and error via preliminary testing to ensure that the tissue was degrading but not dissolving completely. After the treatment, the mass and volume measurements were taken again to gather final density properties after proteolytic degradation (Fig. 1D).

2.4. Mechanical testing

All mechanical testing was performed within 48 h of tissue harvest. Following treatment, the thickness of the gauge length region of each dumbbell-shaped sample was measured optically with a ruler (Gueldner et al., 2023) then was clamped on each end to create a rectangular gauge length of approximately 30 mm in an Instron uniaxial tensile tester (model 5543A, Norwood, MA) (Fig. 1E). The Instron had a 25 N load cell with 0.01 mN resolution, and displacement was measured as grip-to-grip distance with a resolution of 0.02 mm. Raw force versus displacement data of the quasistatic load was collected at a constant displacement rate of 9 mm/min until failure. Following testing, the raw data was analyzed using a MATLAB (MathWorks Inc., Natick, MA) program code in which the uniaxial first Piola-Kirchoff stress (P_{11}) was calculated as $P_{11} = f/a_0$, where f is the force at a given point recorded by the load cell and a_0 as

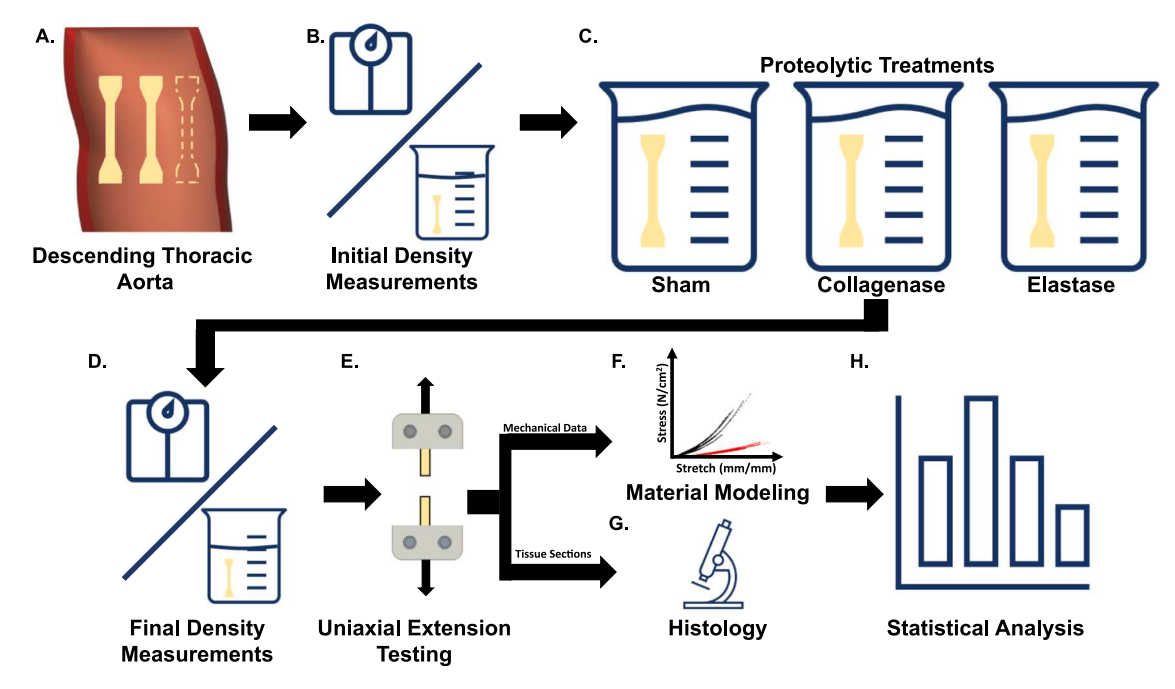


Fig. 1. Treatment protocol of porcine aortic samples. A) Paired axially-oriented thoracic aortic tissue sections were removed from the intact aorta. B) Initial density measurements were taken for each specimen, then they were randomly selected for C) treatment – either sham, collagenase, or elastase – followed by D) a secondary density measurement. E) Each specimen was then mechanically tested to failure via uniaxial extension and the F) data used for curve fitting and property assessment. G) The tissue was then processed for protein histology. Lastly, H) all data were analyzed statistically.

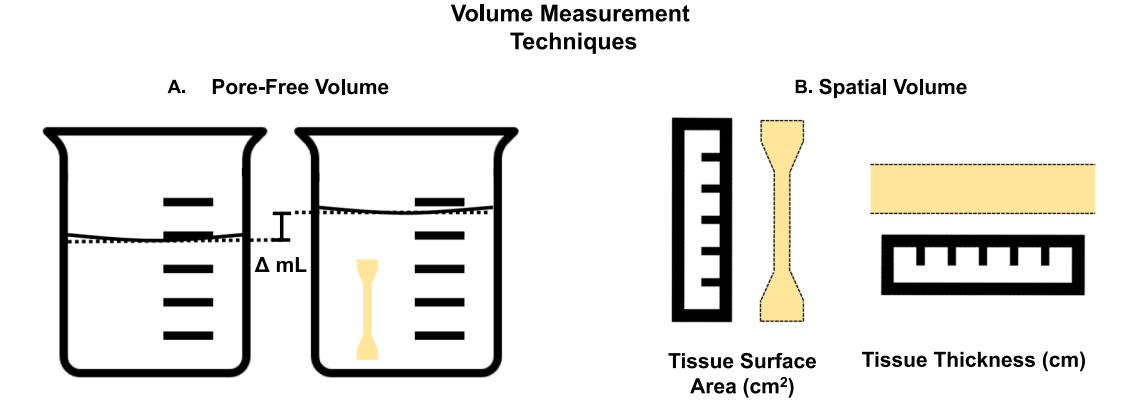


Fig. 2. Techniques used to measure tissue specimen volume. A) "Pore-free volume" was measured by submerging the specimen in phosphate buffered saline to permit filling the pores of the tissue, while B) "spatial volume" measured the geometric space the entire specimen (solid + pores) took up.

cross-sectional area of the aorta specimen calculated by multiplying the initial sample width (4 mm) by the measured initial sample thickness. Ultimate tensile strength was calculated as the maximum stress exhibited before failure. The tangent modulus was determined by measuring the slope of the high stretch region of the stress/stretch curve chosen at a stretch of 0.2 prior to the peak/ultimate stretch.

2.5. Material modeling

Aortic tissue is anisotropic (Liu et al., 2019). However, as a first approximation for the tissue that is commonly adopted to describe tissue response (Luo et al., 2016; Man et al., 2018). Stress/stretch curves for the porcine specimens were imported for each specimen and analyzed independently (sham vs. collagenase vs. elastase) (Fig. 1F). These stress-stretch curves were fit with a two parameter hyperelastic isotropic material model proposed by Raghavan and Vorp (Raghavan and Vorp, 2000) and widely used for aortic tissue across the field (Georgakarakos et al., 2010; Kleinstreuer and Li, 2006; Li et al., 2008; Maier et al., 2010;

Truijers et al., 2007; Venkatasubramaniam et al., 2004):

$$W = \alpha (I_B - 3) + \beta (I_B - 3)^2 \tag{1}$$

where I_B is the first invariant of the left Cauchy-Green tensor B. The material properties α and β were determined by nonlinear least square curve fitting using the least square curve fit MATLAB function, *lsqcurvefit*.

2.6. Insoluble elastin and collagen staining with Movat's Pentachrome

Frozen samples were embedded in Scigen Tissue-Plus Optimal Cutting Temperature Compound embedding medium for frozen tissue specimens (Thermo Fisher Scientific, Waltham, MA). Samples came from the central region of the mechanical specimen, outside the grips and close to but not at the location of failure. Samples were sectioned longitudinally into 5-µm sections and stained by the McGowan Institute Histology Core Laboratory (McGowan Institute for Regenerative

Medicine, University of Pittsburgh, PA). Movat's Pentachrome staining was used to label collagen and elastic fibers in the same sample. All samples were imaged using a Nikon e800 and processed with NIS Elements Software (Nikon, Melville, NY).

2.7. Statistical analysis

All statistical analysis was performed in Prism (GraphPad, San Diego, CA) (Fig. 1H). Data was checked for normality using the Shapiro-Wilk test and for heteroskedasticity using the Breusch-Pagan Test. Repeated measures one-way analysis of variance (ANOVA) with Dunnett's post hoc (with sham as the control group) was used for comparisons of the density measurements and mechanical properties of the three groups of aortic specimens. Simple linear regression was used to calculate R^2 , root mean squared error (RMSE), and p-values. Comparisons of material property fit parameters were analyzed using a Mann-Whitney U-Test. All results are presented as mean \pm standard deviation.

3. Results

3.1. Porcine aortic mass, volume and density measurements

For the aortic specimen groups, there was a significant change in percent mass loss in both the collagenase ($-14.2\pm4.3~\%,~p=0.005$) and elastase groups ($-6.4\pm2.8~\%,~p=0.011$) compared to the sham group (-3.2 \pm 2.1%) (Fig. 3A). The percent-change of pore-free volume (Fig. 3B) was not significantly different between collagenase ($-16.9\pm9.78~\%,~p=0.13$) or elastase ($-6.71\pm4.74~\%,~p=0.44$) groups compared to sham ($-2.25\pm9.90~\%$). The percent-change of pore-free density (Fig. 3C) was also not significantly different between collagenase (4.05 \pm 10.3 %, p = 0.75) or elastase (0.46 \pm 5.55 %, p = 0.99) groups versus sham ($-0.05\pm8.72~\%$).

The percent-change in spatial volume (Fig. 3D) in collagenase-treated (-2.37 ± 7.07 %, p = 0.72) specimens were no different than that of sham (-5.19 ± 5.22 %) specimens. However, that for elastase-treated specimens (3.74 \pm 8.02 %, p = 0.02) was significantly different from the sham group. The percent-change of spatial density (Fig. 3E) between both collagenase (-11.8 ± 5.70 %, p = 0.02) and

Density Measurements

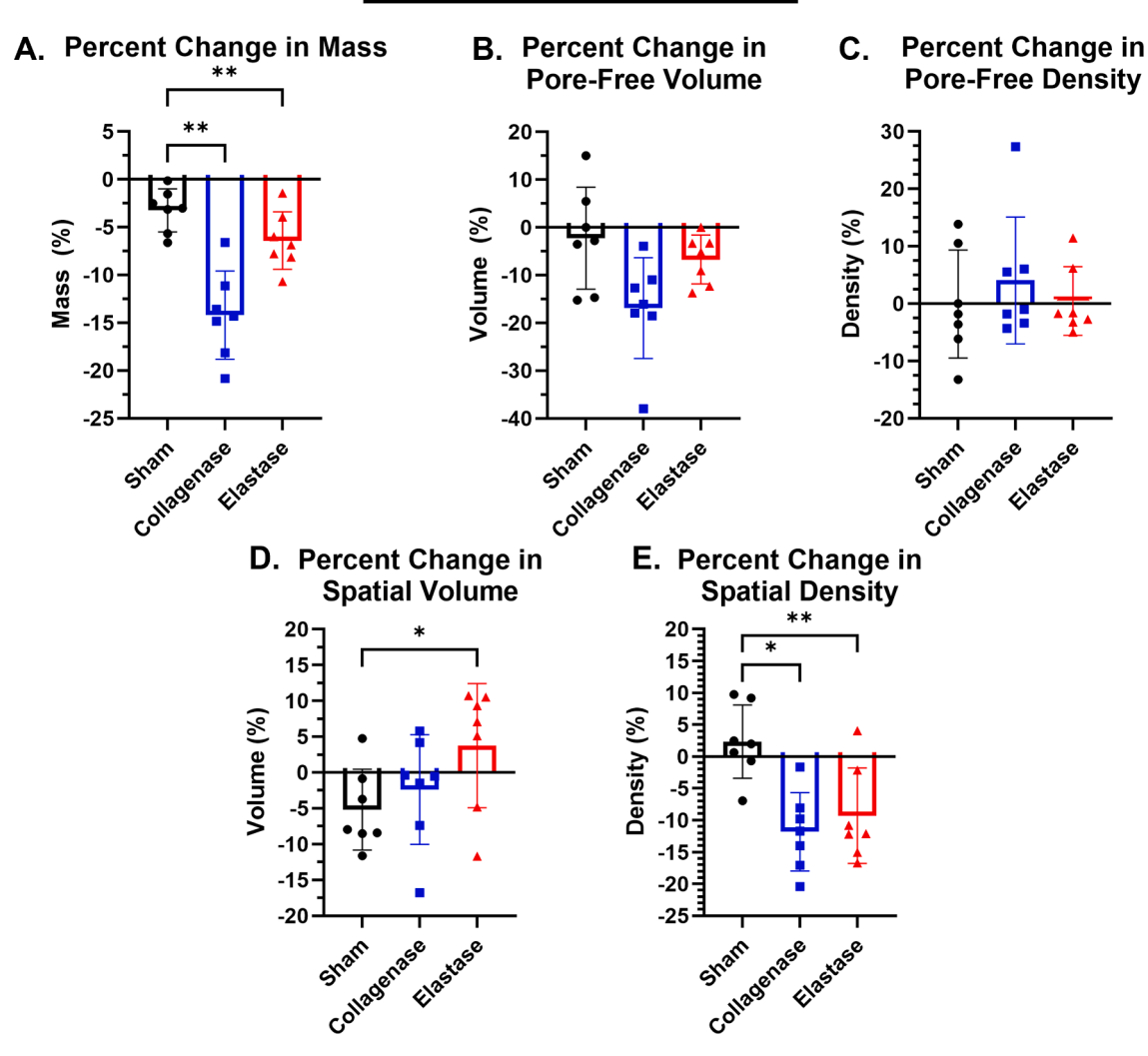


Fig. 3. Density measurements of porcine samples. A) There was a statistically significant difference in mass, B) no significant change in pore-free volume, C) no significant difference in percent change in pore-free density between treatment groups. There was a significant difference in D) spatial volume measurement and E) percent change in spatial density. Bars indicate mean and the error bars indicate standard deviation, while the black circles represent values from individually tested sham specimens, blue squares represent collagenase-treated specimens, and red triangles represent elastase-treated specimens, * indicates p < 0.05, ** indicates p < 0.01.

elastase (-9.29 ± 6.92 %, p=0.003) groups was significantly different than that for sham (2.34 \pm 5.34 %).

3.2. Porcine aortic mechanical properties

The proteolytic treatments each had effects on the mechanical properties of the aortic tissue specimens. The ultimate strength (Fig. 4A) was decreased in both collagenase (63.46 \pm 16.19 N/cm², p = 0.02) and elastase (69.92 \pm 15.15 N/cm², p = 0.03) specimens compared to that of the sham (95.70 \pm 12.89 N/cm²). The tangent modulus (Fig. 4B) also decreased in the collagenase (74.78 \pm 11.09 N/cm², p = 0.007) and elastase (90.77 \pm 25.04 N/cm², p = 0.03) groups compared to that of the sham (149.52 \pm 30.67 N/cm²).

3.3. Correlation between density and mechanical properties

When simple linear regression was used to compare the percent change of spatial density to the ultimate tensile strength, a significant direct correlation was found (p = 0.03, R^2 = 0.2, RMSE = 19.05) (Fig. 4C). Similarly, change in spatial density significantly correlated with tangent modulus (Fig. 4D) (p = 0.02, R^2 = 0.25, RMSE = 36.46).

3.4. Porcine aortic histology

Qualitative inspection of histological images suggests that elastin and collagen are damaged in the tunica media of the collagenase- and elastase-treated groups compared to sham-treated group (Fig. 5), which could explain the observed differences in density (Fig. 3). There were some signs of tissue degradation in sham samples as they were not fixed in paraformaldehyde and left to degrade in PBS at 37 $^{\circ}\text{C}$ which could be indicative of native enzymatic degradation persisting. The tunica adventitia of the sham- and elastase-treated groups consisted of thick collagen bands, whereas the collagenase-treated group showed a markedly thinner collagenous layer.

3.5. Material modeling of porcine tissue

Elastas

The stress/stretch curves and average model fits (Equation (1) for all specimens are shown in Fig. 6A. The material parameter α (Fig. 6B) was (8.26 \pm 4.38 N/cm² for the sham group, 4.56 \pm 1.89 N/cm² for the collagenase group, and 8.01 ± 1.72 N/cm² for the elastase group. There was no significant difference between any of the groups: collagenase vs sham (p = 0.09), elastase vs sham (p = 0.99), or elastasevs collagenase (p = 0.14). For the material parameter β values (Fig. 6C) were (4.47 \pm

Sharin Rase

Elastase

 2.05 N/cm^2 for the sham group, $1.97 \pm 0.32 \text{ N/cm}^2$ for the collagenase group, and $3.27 \pm 1.77 \text{ N/cm}^2$ for the elastase group), there was a difference between the collagenase group compared to the sham (p = 0.04), but there was no difference between the elastase vs sham (p = 0.90) or the elastase vs collagenase groups (p = 0.46). The average model fits had R^2 of 0.99 for sham, R^2 of 0.88 for collagenase-treated, and R^2 of 0.99 for elastase-treated.

4. Discussion

The present study demonstrates for the first time a direct relationship between the spatial density of porcine aorta and its mechanical properties (Fig. 4). Specifically, we found a significant reduction in both tensile strength and tangent modulus resulting from protease treatment along with a concomitant reduction in tissue spatial density (Fig. 3). Overall, this observation suggests that by removing critical proteins from the extracellular matrix, we were able to alter tissue properties and support our overall hypothesis that tissue density reduction is associated with reduced tissue tensile strength in the axial direction. The degree at which a density change is significant enough to impact clinical outcomes remains to be seen. In-vivo density differences - either spatially or temporally - may be more minute and based on ultrastructural alterations rather than what we tested in this paper. Ultrastructural imperfections may nonetheless create points of local weakness for failure to initiate. This may be crucial in developing a new understanding of the structural pathways leading to aortic tissue failure, which would be central in developing new techniques to assess the risk of clinical catastrophes due to, for example, aneurysmal rupture and aortic dissection. We envisage that new clinical imaging techniques may be developed around the assessment of in-vivo tissue density.

Aortic specimens underwent a significant decrease in mass as a result of proteolytic degradation (Fig. 3A). This decrease in mass was linearly correlated with the reduction of pore-free volume (see Supplemental Fig. 1). This suggests that as mass decreases, the pores increase in size, allowing more fluid to flow between the pores than in the initial measurements. This resulted in no change in density when using pore-free volume (Fig. 3C). Spatial volume, on the other hand, remained relatively unchanged in the sham and collagenase groups, but increased in the elastase samples (Fig. 3D). There was a significant decrease in spatial density for both collagenase and elastase treatments (Fig. 3E). This supports the postulate that proteolytic treatments can impact the density of specimens.

In cellular therapy techniques to treat aneurysms, there is a widespread effort to reestablish vascular constituent normalcy by reverting

25 -20 -15 -10 -5

Percent Change in Spatial Density (%)

10 15 20

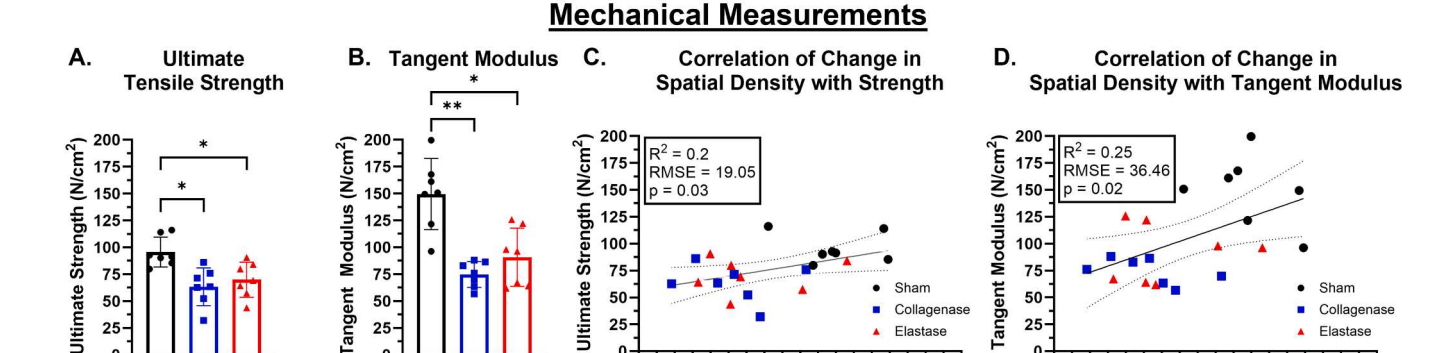


Fig. 4. Mechanical results. There was a significant difference for aortic tissue samples across treatment groups in A) ultimate strength and B) tangent modulus. Comparing C) percent change in spatial density with C) strength and D) tangent modulus revealed significant direct correlations. Bars indicate mean and the error bars indicate standard deviation, while the black circles represent values from individually tested sham specimens, blue squares represent collagenase-treated specimens, and red triangles represent elastase-treated specimens, * indicates p < 0.05, ** indicates p < 0.01.

-20 -15 -10 -5

0

Percent Change in Spatial Density (%)

10 15 20

Movat's Pentachrome Staining of Porcine Aorta

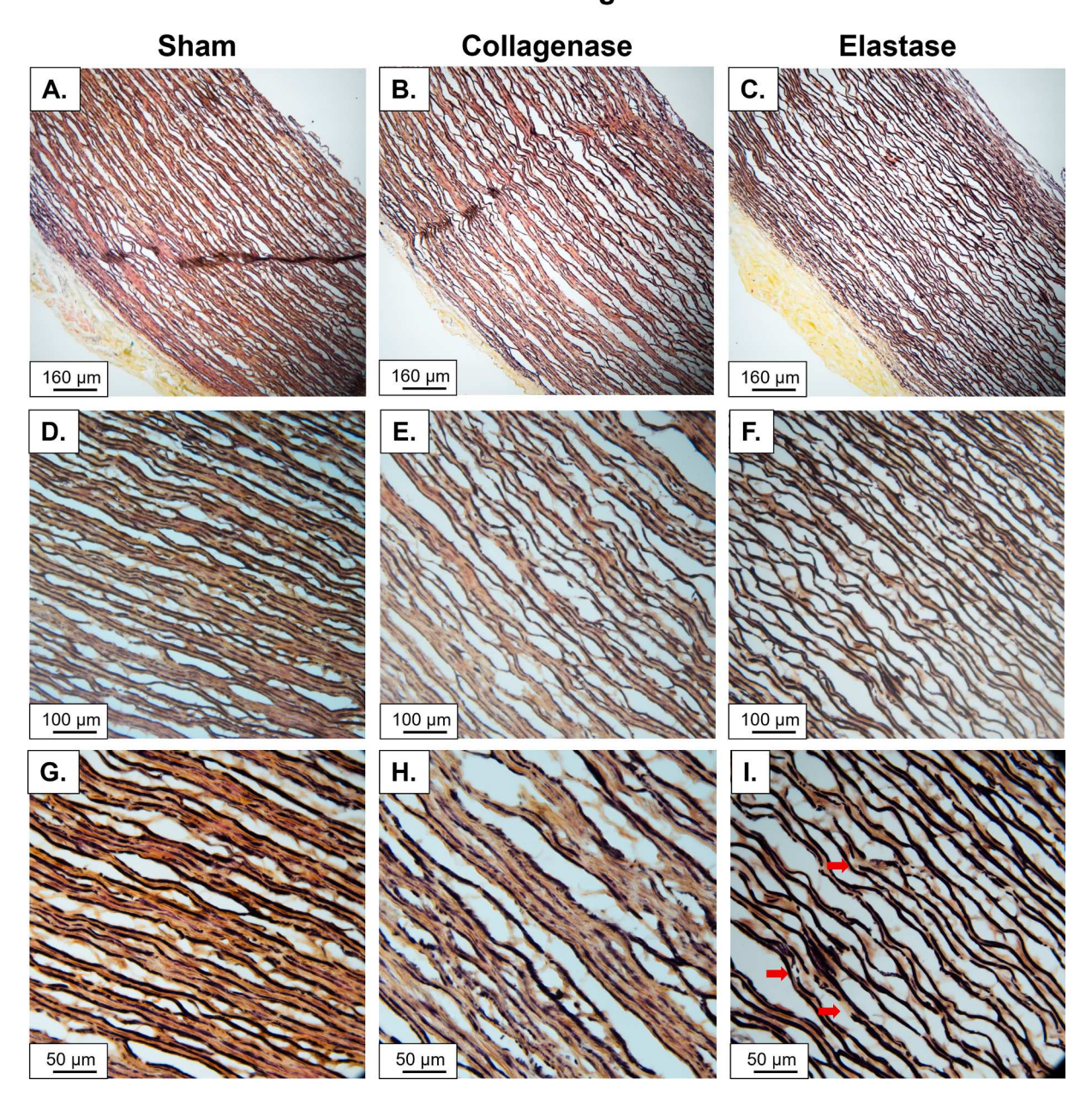


Fig. 5. Histological images of sham- (A, D, G), collagenase- (B, E, H) and elastase-treated (C, F, I) samples from a representative porcine aorta stained with Movat's Pentachrome. Yellow indicates collagen fibers, black indicates elastin fibers, and red indicates fibrin. The sham-treated sample shows fewer breaks of the black elastic fibers, a denser region of yellow collagen between elastic fibers. The collagenase-treated sample shows less collagen content than the sham with a looseness between the fiber bundles. The elastase-treated sample shows marked disruption of black elastic fibers (red arrows in (I)) and less collagen compared to the other two groups.

the collagen and elastin disruption to its pre-aneurysmal state (Blose et al., 2014; Nosoudi et al., 2015; Simionescu et al., 2020). Our results showing changes in aortic tissue properties due to proteolytic treatments are consistent with previous reports (Dobrin et al., 1984; Dobrin and Canfield, 1984; Roach and Burton, 1957; Song and Roach, 1998). In terms of mechanical properties, Davarani et al., noted altered biaxial mechanics in porcine thoracic aorta resulting from elastin and collagen structural changes induced by elastase treatment (Zeinali-Davarani et al., 2013). Noble et al. created a mathematical model to quantify changes to the mechanical response of porcine aortic tissue treated with collagenase and elastase (Noble et al., 2016) and also showed decreased treated tissue strengths in both axial and circumferential orientations. They additionally showed, as has been shown previously, that stiffness

and strength is higher in the circumferential direction. In this paper we have only analyzed the axial direction, a limitation of the current study. Future work should explore correlations the circumferential direction as well as with tissue stiffness parameters derived from biaxial testing of the tissue. Schriefl et al. created a damage model to characterize structural changes in human abdominal aortic tissue at low-strain and high-strain regions using elastase and collagenase treatments, respectively (Schriefl et al., 2015).

While we also quantify in this current study the effect of protease treatments on aortic tissue biomechanical properties, what sets it apart is that we also demonstrate effects on tissue density and report a potentially new finding that aortic tissue density is significantly and directly correlated with both ultimate tensile strength and tangent

Raghavan-Vorp Model Fit

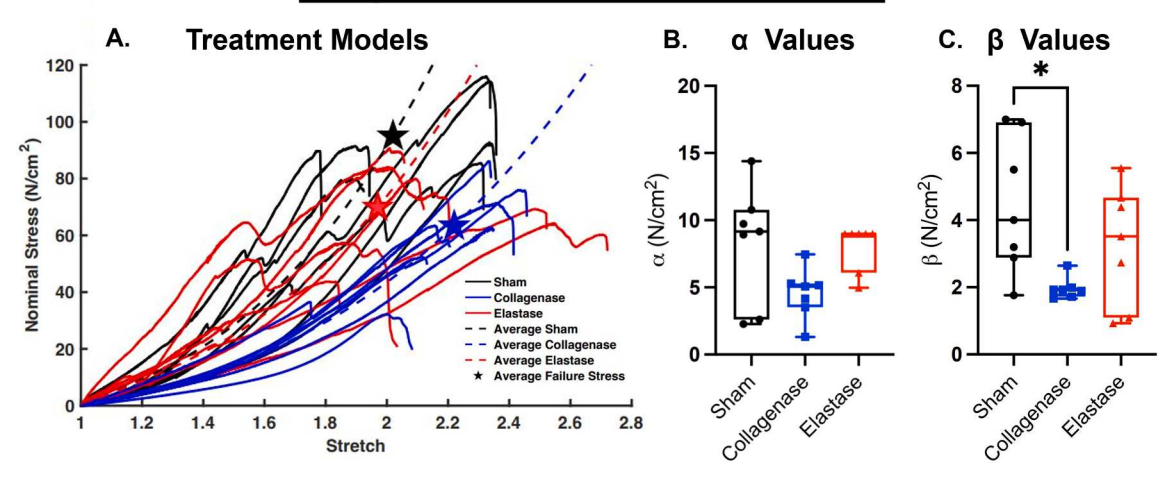


Fig. 6. A) Raw experimental stress strain data (solid lines) and best fits of the Raghavan-Vorp model (equation (1). There was no significant difference in the material parameter α between groups (B), while β was significantly lower in collagenase-treated tissue compared to sham, with no difference compared to elastase-treated values (C). The box and whisker plots show the median line, 25th and 75th percentiles create the box and the whiskers are at the minimum and maximum values.

modulus. To our knowledge a relationship between the density of soft tissues and their mechanical strength has not previously been reported. We also demonstrated a novel experimental technique to determine tissue density *ex-vivo* by applying the concepts of volume presented by Archimedes. Our technique enabled us to account for pore-free volume of the tissue and revealed that while spatial volume remained unchanged, pore-free volume decreased linearly with mass. In future work, we plan to take anisotropy into account in our material modeling.

Our study had the following limitations. Since the tissue was removed from the body, the testing neglected the effects of the surrounding tissues. Histologic imaging showed spatially heterogeneous degradation of the tissue structure from both collagenase and elastase treatment resulting in increased fraction of pores within the tissue (Fig. 5) that in turn manifested in reduced spatial densities of treated tissues. Collagenase and elastase treatment has other effects than density reduction, such as fragmentation of elastin, which could also change the strength or the stiffness of the tissue (Trabelsi et al., 2020). This should be considered in future work. We took the tissue in this study to be isotropic but it aortic aneurysm tissue is anisotropic (Liu et al., 2019), which should be considered if biaxial testing was employed. While our study encapsulates full tear failure, which correctly examines rupture, this is not a failure mode consistent with aortic dissection, which is commonly associated with a partial tear. This study looks strictly at the effects longitudinally, which has been shown to be weaker than the circumferential direction (Guinea et al., 2010), and would be interesting to explore in future work. Additionally, our methods were limited to using a single bulk tissue density measurement for a given tissue specimen for comparison to its tensile strength, as more refined measurements of density have not yet been discovered, tested, or validated. We envisage that such spatial variations in density play a significant role in the damage initiation and propagation at the microstructural level leading to the loss of tissue biomechanical integrity. Indeed, in an earlier computational study we showed that collagen fibers create microstructural "stress paths" within the tissue when subjected to uniaxial loading conditions, and principal stresses were significantly higher in the zones of lower fiber density (Thunes et al., 2016). We are currently performing further experimental and computational studies to elucidate the effect of such spatial heterogeneities on tissue failure biomechanics.

5. Conclusions

This work demonstrates for the first time that aortic tissue stiffness and tensile strength are directly correlated with tissue density when altered by proteolytic enzymes. These findings could possibly be leveraged to develop an enhanced understanding of tissue failure biomechanics with potential implications to clinical care. For example, with respect to aortic aneurysms, a means to non-invasively assess tissue density could serve as a proxy to tissue tensile strength, which could lead to improved evidence-based aortic wall rupture surveillance management protocols over the current practice of relying on orthogonal dimensional measurements alone.

Declaration of competing interest

The authors declare that they have no known competing financial interests or personal relationships that could have appeared to influence the work reported in this paper.

Acknowledgements

We would like to acknowledge support (for P.G. and K.R.) by the National Science Foundation (P.G. for the Graduate Research Fellowship Program under Grant No. 1747452). Any opinions, findings, and conclusions or recommendations expressed in this material are those of the author(s) and do not necessarily reflect the views of the National Science Foundation. Additionally, we would like to acknowledge support (for I. K.M.C.), from the NIBIB training grant 'Cellular Approaches to Tissue Engineering and Regeneration (T32 EB001026), and (for E.A.) by the Frederick Honors College at the University of Pittsburgh for the Brackenridge Fellowship.

Appendix A. Supplementary data

Supplementary data to this article can be found online at https://doi.org/10.1016/j.jbiomech.2024.112226.

References

Alagappan, P., Rajagopal, K., Kannan, K., 2018a. A damage initiation criterion for a class of viscoelastic solids. Proceedings of the Royal Society A: Mathematical, Physical and Engineering Sciences 474, 20180064.

Alagappan, P., Kannan, K., Rajagopal, K., 2016. On a possible methodology for identifying the initiation of damage of a class of polymeric materials. Proc. Roy. Soc. A: Math. Phys. Eng. Sci. 472, 20160231.

Alagappan, P., Rajagopal, K., 2022. Prediction of the Onset of Failure in Elastomeric Solids With Weld Lines Being Represented as Localized Regions of Lower Density. J. Eng. Mater. Technol. 144.

- Alagappan, P., Rajagopal, K., 2023. Fatigue in a class of viscoelastic solids. Forces Mech. 10. 100169.
- Alagappan, P., Rajagopal, K., Kannan, K., 2018. Initiation of damage in a class of polymeric materials embedded with multiple localized regions of lower density. Math. Mech. Solids 23, 865–878.
- Berman, A.G., Romary, D.J., Kerr, K.E., Gorazd, N.E., Wigand, M.M., Patnaik, S.S., Finol, E.A., Cox, A.D., Goergen, C.J., 2022. Experimental aortic aneurysm severity and growth depend on topical elastase concentration and lysyl oxidase inhibition. Sci Rep 12, 99.
- Blose, K.J., Ennis, T.L., Arif, B., Weinbaum, J.S., Curci, J.A., Vorp, D.A., 2014. Periadventitial adipose-derived stem cell treatment halts elastase-induced abdominal aortic aneurysm progression. Regen Med 9, 733–741.
- Chung, T.K., Kim, J., Gueldner, P.H., Vorp, D.A., 2024. A Comparative Study of Machine Learning and Algorithmic Approaches to Automatically Identify the Yield Point in Normal and Aneurysmal Human Aortic Tissues. J. Biomech. Eng. 146.
- Darling, R.C., Messina, C.R., Brewster, D.C., Ottinger, L.W., 1977. Autopsy study of unoperated abdominal aortic aneurysms. The case for early resection. Circulation 56, III61-164
- Davies, R.R., Goldstein, L.J., Coady, M.A., Tittle, S.L., Rizzo, J.A., Kopf, G.S., Elefteriades, J.A., 2002. Yearly rupture or dissection rates for thoracic aortic aneurysms: simple prediction based on size. Ann. Thorac. Surg. 73, 17–28.
- Di Martino, E.S., Bohra, A., Vande Geest, J.P., Gupta, N., Makaroun, M.S., Vorp, D.A., 2006. Biomechanical properties of ruptured versus electively repaired abdominal aortic aneurysm wall tissue. J. Vasc. Surg. 43, 570–576.
- Dobrin, P.B., Canfield, T.R., 1984. Elastase, collagenase, and the biaxial elastic properties of dog carotid artery. Am. J. Physiol.-Heart Circul. Physiol. 247, H124–H131.
- Dobrin, P.B., Baker, W.H., Gley, W.C., 1984. Elastolytic and collagenolytic studies of arteries: implications for the mechanical properties of aneurysms. Arch. Surg. 119, 405–409.
- Dobrin, P.B., Schwarcz, T., Baker, W., 1988. Mechanisms of arterial and aneurysmal tortuosity. Surgery 104, 568–571.
- Duprey, A., Trabelsi, O., Vola, M., Favre, J.-P., Avril, S., 2016. Biaxial rupture properties of ascending thoracic aortic aneurysms. Acta Biomater. 42, 273–285.
- Ferreira, J., Parente, M., Jorge, R., 2017. Modeling of soft tissues with damage.

 Proceedings of the Institution of Mechanical Engineers, Part I: Journal of Materials:

 Design and Applications 231, 131–139.
- Fung, Y.C., 1991. What are the residual stresses doing in our blood vessels? Ann. Biomed. Eng. 19, 237–249.
- Fung, Y., Liu, S., 1991. Changes of zero-stress state of rat pulmonary arteries in hypoxic hypertension. J. Appl. Physiol. 70, 2455–2470.
- Gasser, T.C., Ogden, R.W., Holzapfel, G.A., 2006. Hyperelastic modelling of arterial layers with distributed collagen fibre orientations. J. R. Soc. Interface 3, 15–35.
- Gee, M., Reeps, C., Eckstein, H., Wall, W., 2009. Prestressing in finite deformation abdominal aortic aneurysm simulation. J. Biomech. 42, 1732–1739.
- Georgakarakos, E., Ioannou, C., Kamarianakis, Y., Papaharilaou, Y., Kostas, T., Manousaki, E., Katsamouris, A., 2010. The role of geometric parameters in the prediction of abdominal aortic aneurysm wall stress. Eur. J. Vasc. Endovasc. Surg. 39, 42–48
- Gloviczki, P., Pairolero, P.C., Mucha Jr, P., Farnell, M.B., Hallett Jr, J.W., Ilstrup, D.M., Toomey, B.J., Weaver, A.L., Bower, T.C., Bourchier, R.G., 1992. Ruptured abdominal aortic aneurysms: repair should not be denied. J. Vasc. Surg. 15, 851–859.
- Gueldner, P.H., Marini, A.X., Li, B., Darvish, C.J., Chung, T.K., Weinbaum, J.S., Curci, J. A., Vorp, D.A., 2023. Mechanical and matrix effects of short and long-duration exposure to BAPN in elastase-induced model AAA in mice. JVS-Vascular. Science 100098
- Guinea, G.V., Atienza, J.M., Rojo, F.J., García-Herrera, C.M., Yiqun, L., Claes, E., Goicolea, J.M., García-Montero, C., Burgos, R.L., Goicolea, F.J., 2010. Factors influencing the mechanical behaviour of healthy human descending thoracic aorta. Physiol. Meas. 31, 1553.
- He, C.M., Roach, M.R., 1994. The composition and mechanical properties of abdominal aortic aneurysms. J. Vasc. Surg. $20,\,6-13$.
- Hinton, M., Kaddour, A.S., Soden, P.D., 2004. Failure criteria in fibre reinforced polymer composites: the world-wide failure exercise. Elsevier.
- Karimi, A., Navidbakhsh, M., Razaghi, R., 2014. Plaque and arterial vulnerability investigation in a three-layer atherosclerotic human coronary artery using computational fluid-structure interaction method. J. Appl. Phys. 116.
- Kleinstreuer, C., Li, Z., 2006. Analysis and computer program for rupture-risk prediction of abdominal aortic aneurysms. Biomed. Eng. Online 5, 1–13.
- Kontopodis, N., Pantidis, D., Dedes, A., Daskalakis, N., Ioannou, C.V., 2016. The–not so–solid 5.5 cm threshold for abdominal aortic aneurysm repair: facts, misinterpretations, and future directions. Front. Surg. 3, 1.
- Korenczuk, C.E., Votava, L.E., Dhume, R.Y., Kizilski, S.B., Brown, G.E., Narain, R., Barocas, V.H., 2017. Isotropic failure criteria are not appropriate for anisotropic fibrous biological tissues. J. Biomech. Eng. 139, 071008.
- Lau, C., Leonard, J.R., Iannacone, E., Gaudino, M., Girardi, L.N., Year Surgery for acute presentation of thoracoabdominal aortic disease. In Seminars in thoracic and cardiovascular surgery.
- Li, Z.-Y., Jean, U., Tang, T.Y., Soh, E., See, T.C., Gillard, J.H., 2008. Impact of calcification and intraluminal thrombus on the computed wall stresses of abdominal aortic aneurysm. J. Vasc. Surg. 47, 928–935.
- Liu, S., Fung, Y., 1988. Zero-stress states of arteries.
- Liu, S., Fung, Y., 1989. Relationship between hypertension, hypertrophy, and opening angle of zero-stress state of arteries following aortic constriction.
- Liu, M., Liang, L., Sulejmani, F., Lou, X., Iannucci, G., Chen, E., Leshnower, B., Sun, W., 2019. Identification of in vivo nonlinear anisotropic mechanical properties of

- ascending thoracic aortic aneurysm from patient-specific CT scans. Sci. Rep. 9, 12983.
- Lombardi, J.V., Hughes, G.C., Appoo, J.J., Bavaria, J.E., Beck, A.W., Cambria, R.P., Charlton-Ouw, K., Eslami, M.H., Kim, K.M., Leshnower, B.G., 2020. Society for Vascular Surgery (SVS) and Society of Thoracic Surgeons (STS) reporting standards for type B aortic dissections. Ann. Thorac. Surg. 109, 959–981.
- Lu, J., Zhou, X., Raghavan, M.L., 2007. Inverse elastostatic stress analysis in predeformed biological structures: demonstration using abdominal aortic aneurysms. J. Biomech. 40, 693–696.
- Luo, Y., Duprey, A., Avril, S., Lu, J., 2016. Characteristics of thoracic aortic aneurysm rupture in vitro. Acta Biomater. 42, 286–295.
- Maier, A., Gee, M., Reeps, C., Pongratz, J., Eckstein, H.-H., Wall, W., 2010. A comparison of diameter, wall stress, and rupture potential index for abdominal aortic aneurysm rupture risk prediction. Ann. Biomed. Eng. 38, 3124–3134.
- Man, V., Polzer, S., Gasser, T.C., Novotny, T., Bursa, J., 2018. Impact of isotropic constitutive descriptions on the predicted peak wall stress in abdominal aortic aneurysms. Med. Eng. Phys. 53, 49–57.
- Marbacher, S., Marjamaa, J., Bradacova, K., Von Gunten, M., Honkanen, P., Abo-Ramadan, U., Hernesniemi, J., Niemelä, M., Frösen, J., 2014. Loss of mural cells leads to wall degeneration, aneurysm growth, and eventual rupture in a rat aneurysm model. Stroke 45, 248–254.
- Mohan, D., Melvin, J.W., 1983. Failure properties of passive human aortic tissue. II—Biaxial tension tests. J. Biomech. 16, 31–44.
- Mousavi, S.J., Farzaneh, S., Avril, S., 2018. Computational predictions of damage propagation preceding dissection of ascending thoracic aortic aneurysms. International Journal for Numerical Methods in Biomedical Engineering 34, e2944.
- Nelson, S.J., Creechley, J.J., Wale, M.E., Lujan, T.J., 2020. Print-A-Punch: A 3D printed device to cut dumbbell-shaped specimens from soft tissue for tensile testing. J. Biomech. 112, 110011.
- Noble, C., Smulders, N., Green, N.H., Lewis, R., Carré, M.J., Franklin, S.E., MacNeil, S., Taylor, Z.A., 2016. Creating a model of diseased artery damage and failure from healthy porcine aorta. Journal of the Mechanical Behavior of Biomedical Materials 60, 378–393.
- Nosoudi, N., Nahar-Gohad, P., Sinha, A., Chowdhury, A., Gerard, P., Carsten, C.G., Gray, B.H., Vyavahare, N.R., 2015. Prevention of abdominal aortic aneurysm progression by targeted inhibition of matrix metalloproteinase activity with batimastat-loaded nanoparticles. Circ Res 117, e80–e89.
- Özkaya, N., Leger, D., Goldsheyder, D., Nordin, M., 2016. Fundamentals of biomechanics: equilibrium, motion, and deformation. Springer
- Raghavan, M.L., Vorp, D.A., 2000. Toward a biomechanical tool to evaluate rupture potential of abdominal aortic aneurysm: identification of a finite strain constitutive model and evaluation of its applicability. J. Biomech. 33, 475–482.
- Raghavan, M.L., Webster, M.W., Vorp, D.A., 1996. Ex vivo biomechanical behavior of abdominal aortic aneurysm: assessment using a new mathematical model. Ann Biomed Eng 24, 573–582.
- Rausch, M., Karniadakis, G., Humphrey, J., 2017. Modeling soft tissue damage and failure using a combined particle/continuum approach. Biomech. Model. Mechanobiol. 16, 249–261.
- Roach, M.R., Burton, A.C., 1957. The reason for the shape of the distensibility curves of arteries. Can. J. Biochem. Physiol. 35, 681–690.
- Schriefl, A.J., Schmidt, T., Balzani, D., Sommer, G., Holzapfel, G.A., 2015. Selective enzymatic removal of elastin and collagen from human abdominal aortas: Uniaxial mechanical response and constitutive modeling. Acta Biomaterialia 17, 125–136.
- Siika, A., Bogdanovic, M., Liljeqvist, M.L., Gasser, T.C., Hultgren, R., Roy, J., 2023. Three-dimensional growth and biomechanical risk progression of abdominal aortic aneurysms under serial computed tomography assessment. Scientific Reports 13, 2283
- Simionescu, D., Casco, M., Turner, J., Rierson, N., Yue, J., Ning, K., 2020. Chemical stabilization of the extracellular matrix attenuates growth of experimentally induced abdominal aorta aneurysms in a large animal model. JVS-Vascular Science 1, 69–80.
- Sokolis, D.P., 2015. Effects of aneurysm on the directional, regional, and layer distribution of residual strains in ascending thoracic aorta. J. Mech. Behav. Biomed. Mater. 46, 229–243.
- Sokolis, D.P., Markidi, D.C., Iliopoulos, D.C., Kourkoulis, S.K., 2023. Residual strains in ascending thoracic aortic aneurysms: The effect of valve type, layer, and circumferential quadrant. J. Biomech. 147, 111432.
- Song, S.-H., Roach, M.R., 1998. The Effects of Aging and Atherosclerosis on Elastin of Human Aortas; Quantitative Analysis of Elastin-Content and SEM Analysis of Elastolysis. Kor. J. Physiol. Pharmacol. 2, 591–600.
- Thunes, J.R., Pal, S., Fortunato, R.N., Phillippi, J.A., Gleason, T.G., Vorp, D.A., Maiti, S., 2016. A structural finite element model for lamellar unit of aortic media indicates heterogeneous stress field after collagen recruitment. J. Biomech. 49, 1562–1569.
- Thunes, J.R., Phillippi, J.A., Gleason, T.G., Vorp, D.A., Maiti, S., 2018. Structural modeling reveals microstructure-strength relationship for human ascending thoracic aorta. J. Biomech. 71, 84–93.
- Trabelsi, O., Dumas, V., Breysse, E., Laroche, N., Avril, S., 2020. In vitro histomechanical effects of enzymatic degradation in carotid arteries during inflation tests with pulsatile loading. J. Mech. Behav. Biomed. Mater. 103, 103550.
- Truijers, M., Pol, J., Schultzekool, L., Van Sterkenburg, S., Fillinger, M., Blankensteijn, J., 2007. Wall stress analysis in small asymptomatic, symptomatic and ruptured abdominal aortic aneurysms. Eur. J. Vasc. Endovasc. Surg. 33, 401–407.
- Vande Geest, J.P., Di Martino, E.S., Bohra, A., Makaroun, M.S., Vorp, D.A., 2006a.
 A Biomechanics-Based Rupture Potential Index for Abdominal Aortic Aneurysm Risk Assessment. Ann. N. Y. Acad. Sci. 1085, 11–21.
- Vande Geest, J.P., Sacks, M.S., Vorp, D.A., 2006b. The effects of aneurysm on the biaxial mechanical behavior of human abdominal aorta. J. Biomech. 39, 1324–1334.

- Vande Geest, J.P., Wang, D.H., Wisniewski, S.R., Makaroun, M.S., Vorp, D.A., 2006c. Towards a noninvasive method for determination of patient-specific wall strength distribution in abdominal aortic aneurysms. Ann Biomed Eng 34, 1098–1106.
- Venkatasubramaniam, A., Fagan, M., Mehta, T., Mylankal, K., Ray, B., Kuhan, G., Chetter, I., McCollum, P., 2004. A comparative study of aortic wall stress using finite element analysis for ruptured and non-ruptured abdominal aortic aneurysms. Eur. J. Vasc. Endovasc. Surg. 28, 168–176.
- Volokh, K., 2011. Modeling failure of soft anisotropic materials with application to arteries. J. Mech. Behav. Biomed. Mater. 4, 1582–1594.
- Volokh, K., Vorp, D., 2008. A model of growth and rupture of abdominal aortic aneurysm. J. Biomech. 41, 1015–1021.
- Vorp, D.A., 2007. Biomechanics of abdominal aortic aneurysm. J. Biomech. 40, 1887–1902.
- Vorp, D.A., Raghavan, M.L., Webster, M.W., 1998. Mechanical wall stress in abdominal aortic aneurysm: Influence of diameter and asymmetry. J. Vasc. Surg. 27, 632–639.
- Zeinali-Davarani, S., Chow, M.-J., Turcotte, R., Zhang, Y., 2013. Characterization of biaxial mechanical behavior of porcine aorta under gradual elastin degradation. Ann. Biomed. Eng. 41, 1528–1538.